Light impurity transport in tokamaks: on the impact of neutral beam fast ions

P. Manas,[1, 2] A. Kappatou,[1] C. Angioni,[1] R. M. McDermott,[1] and the ASDEX Upgrade Team[3]

[1]*Max-Planck-Institut für Plasmaphysik, D-85748 Garching, Germany*
[2]*CEA, IRFM, F-13108 Saint-Paul-lez-Durance, France*
[3]*H. Meyer et al, Nucl. Fusion 59 (2019) 112014*

Previous studies (e.g. [Kappatou *et al* Nuclear Fusion, 2019]) have shown that discrepancies exist between experimental and modelled light impurity peaking in specific regimes. In particular, in NBI heated plasmas, the strong hollowness of boron profiles are not captured by the modelling. In this context, a dedicated ASDEX Upgrade discharge, including boron and helium density measurements, is studied where such discrepancies appear. Emphasis is given to the impact of fast ions on the turbulent and neoclassical impurity transport computed with the codes GKW and NEO respectively. It is shown that fast ions increase the turbulent outward impurity convection via an increase of both thermo- and roto-diffusion. This increase is correlated with the stabilisation of the Ion Temperature Gradient driven mode (ITG). Additionally, the ratio of the turbulent impurity diffusion over the ion heat diffusion is reduced with fast ions, which in turn, increases the neoclassical contributions to the impurity peaking. Finally, neoclassical convection is also enhanced through changes in the ion density gradient due to the modification of the quasi-neutrality condition in the presence of peaked fast ion profiles. The combination of these three mechanisms induced by the fast ion population has a significant impact on the development of hollow boron profiles, up to experimental levels.

PACS numbers:

I. INTRODUCTION

Impurities are inherent to tokamak plasma operation through injection at the edge to mitigate the power on the divertor plates, recycling from the plasma facing components or as the thermalised product of the fusion reaction (helium ash). However, they can have detrimental effects on the plasma, such as fuel dilution and high core radiation. It is then of significant importance to understand theoretically and investigate experimentally impurity transport in order to optimise tokamak plasma operation performance.

Theoretical studies moved from qualitative descriptions of impurity transport based on neoclassical and gyrokinetic theories (e.g. [1, 2]) to accurate, quantitative comparisons with the experiment. This is true for both light [3–8] and heavy impurities [9, 10]. In contrast, recently observed discrepancies between modeled and experimental light impurity radial profiles at the ASDEX Upgrade (AUG) and JET tokamaks are challenging the current theoretical understanding [11–13]. Indeed, in regimes where the normalised ion temperature and toroidal rotation gradients are large and where transient transport mechanisms such as sawteeth and edge localised modes (ELM) are negligible, theory does not quantitatively predict the experimental negative boron/carbon peaking factors (hollow profiles) and in some cases even predict peaked profiles instead [11, 13, 14]. A more detailed experimental analysis of the diffusive and convective parts of the boron flux performed at AUG for low NBI heating cases ($\leq$ 5 MW) [15] showed good agreement with the modelling results [16]. The opposite behaviour is observed for helium where the predicted peaking factors are underestimated [11] at low neutral beam injection heating (NBI). The hollow impurity profiles and the predictions mismatch for different light impurities at high NBI heating are of great relevance for operational purposes and should motivate the search for the missing piece in the theoretical desciption of light impurity transport performed up to now.

This work aims to close the gap between modelling and the experimental light impurity profiles in such regimes by investigating the effect of fast ions on light impurity transport in the framework of neoclassical and local gyrokinetic theory. An AUG discharge, with strong NBI heating and thus large neutral beam fast ions content, is scrutinised in regimes where discrepancies with modelling of impurity transport without fast ions, as done in previous publications, are observed. Extensive linear and nonlinear gyrokinetic simulations including fast ions provide insights on their effect on impurity transport. Their impact on the neoclassical transport is also found to be significant. The resulting impurity peaking factors for boron and helium are then compared to experimental data at mid-radius where it is shown that all the effects of fast ions on the turbulent and neoclassical transport components need to be included in the modelling in order to quantitatively reproduce experimental hollow boron profiles.

The paper is organised as follows. Section II presents the experimental conditions obtained in an AUG discharge with strong NBI heating, together with the experimental radial profiles in 4 stationary phases including those of boron and helium densities. In section III the different impacts of fast ions on turbulent and neoclassical impurity transport are investigated separately. Finally in section IV comparisons are performed between modelled and experimental peaking factors, including all the effects characterised in III and conclusions are drawn on the nature and importance of such effects.

II.   EXPERIMENTAL RESULTS

Discharges dedicated to light impurity transport studies have been carried out at AUG for boron and helium [11, 15]. A wide parameter range was covered by varying the Electron Cyclotron Resonance Heating (ECRH), the Neutral Beam Injection (NBI) and the plasma fuelling. It was found that the local boron peaking factor ($R/L_{n_Z} = -(R/n_Z)\partial n_Z/\partial r$ with R the major radius, n_Z the impurity density and r the minor radius) predictions from gyrokinetic and neoclassical transport simulations, performed at $\rho_{tor} = 0.5$ (normalised toroidal flux coordinate), were inconsistent in regimes where experimental impurity profiles are particularly hollow (high NBI heating powers, low/none ECRH). These discrepancies have also been observed in the JET tokamak with the ITER-like wall and carbon wall [12, 13], suggesting a missing ingredient in the modelling efforts achieved up to now. Additionally, the predicted helium peaking factor in AUG features the opposite trend, that is, at low NBI power, the experimental $R/L_{n_{He}}$ is underestimated while at larger values of NBI power, the predicted and experimental impurity profiles are in quantitative agreement [11]. To tackle these discrepancies, a specific AUG discharge featuring consistent and inconsistent theoretical predictions with respect to experimental observations, is described below and later on further compared against modelling including the neutral beam fast ions.

The H-mode AUG discharge studied throughout this paper was performed at a plasma current of $I_p = 0.6$ MA, a toroidal magnetic field of $B_T = 2.5$ T, a core line averaged electron density of $n_e \sim 4.2 \times 10^{19}$ m^{-3} with two NBI injected power levels (co-current), 7.5 and 10 MW, and with central electron cyclotron resonance heating (ECRH) ranging from 0 to 2.7 MW. For the 10 MW NBI phase, two off-axis (co-current) and two on-axis beams are used whereas for the phase at 7.5 MW of NBI power, one off-axis beam (co-current) is switched off. Throughout the discharge, neutral beam sources are switched on and off (for a constant time averaged heat source), to substract the passive emission from the helium charge exchange spectra [17]. Four stationary phases of 200 ms ($\sim$ 5 confinement times) are investigated and were chosen to include a large range of impurity peaking factors at mid-radius. Indeed, R/L_{n_Z} depends on the main turbulent regime and is defined by convective mechanisms (e.g. [1, 2, 18]): a constant pinch stemming from the magnetic field geometry, thermo and roto-diffusion terms related to the normalised ion temperature gradient R/L_{T_i} and toroidal rotation gradient, respectively ($u' = -(R^2/v_{th})\partial\Omega/\partial r$ with $v_{th} = \sqrt{(2T/m)}$ the thermal velocity and Ω the toroidal rotation frequency). Changing heating power levels deposited on the electrons and ions results in a change of the turbulence characteristics, in particular due to changes in T_e/T_i in this case, but also due to changes in R/L_{T_i}, R/L_{T_e} R/L_n and u' (e.g. flattening of the toroidal rotation profiles with ECRH heating [19]). These changes affect directly
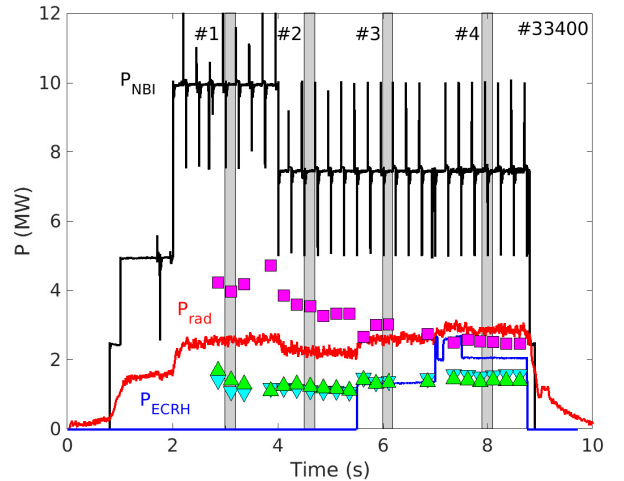

FIG. 1: Total radiated power, NBI and ECRH heating powers in AUG discharge #33400. The studied 200 ms stationary phases are indicated by gray shaded areas. The central ion temperature in keV (squares) and the central boron/helium densities (down/up triangles) in 10^{17} m^{-3} are also shown.

and indirectly the impurity convective terms [3, 11]. The selected time windows for this discharge, as well as the time traces of the radiated and injected power levels are shown in Fig. 1.

Boron and helium density profiles are measured with Charge Exchange Recombination Spectroscopy (CXRS) [17, 20] and fitted together with their respective normalised gradients (peaking factors) in Fig. 2 for the two extreme cases, with and without ECRH heating. The density profiles are shown with 2 standard deviation σ (using the same methodology as in [21]) while the normalised gradients are shown with only 1σ. Due to the lack of measurements at the edge, the unconstrained edge density profiles result in large error bars on the gradients. The local impurity peaking factors at mid-radius are observed to have the strongest variations when going from 0 MW to 2 MW of ECRH in comparison to other radial locations. Helium profiles are observed to go from flat (or slightly hollow) to peaked when ECRH is applied whereas boron goes from particularly hollow to peaked, with a stronger variation of R/L_{n_Z} compared to helium. This large range of R/L_{n_Z} obtained at $r/a = 0.5$ and the transport being unaffected by transient mechanisms such as ELMs (pedestal top at $r/a \sim 0.85$) and sawteeth provides a good testbed for the investigation of possible missing mechanisms in the modelled impurity convective fluxes. Finally it is found that these experimental levels of helium and boron densities are sufficiently low to make use of the trace limit in the rest of the paper for all 4 phases (concentrations below 0.5%). This limit was also tested and found valid in [11, 13].

Background kinetic profiles, and in particular the corresponding gradients, are required for turbulence and neoclassical simulations. In addition, convective impu-
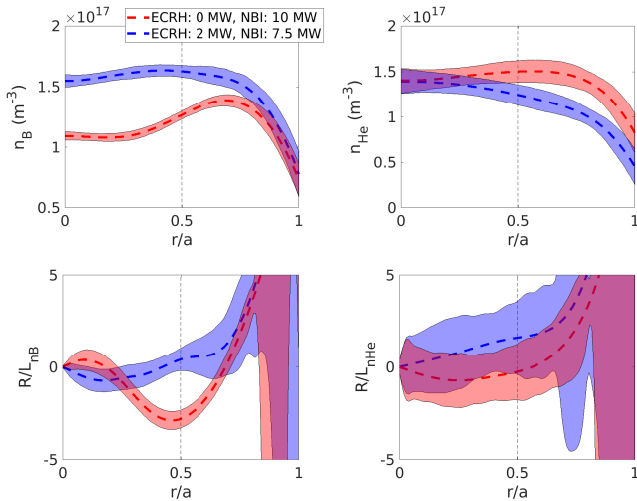
FIG. 2: Fitted radial profiles of boron and helium (top panels) with
2σ error bars for phase #1 and #4 of Fig. 1. The corresponding
normalised gradients are shown with 1σ error bars (bottom panels).

rity fluxes are driven by the ion temperature and the
toroidal rotation gradients. Prior to dedicated gyroki-
netic simulations, these profiles can provide hints on the
turbulence nature and the strength of the convective im-
purity fluxes. The ion temperature and toroidal rota-
tion profiles are measured with CXRS, while the elec-
tron temperature and density profiles are obtained from
Electron Cyclotron Emission and Thomson scattering,
respectively. The magnetic equilibrium is taken from the
code CLISTE [22]. In Fig. 3 the fitted profiles and their
gradients, together with the corresponding error bars are
shown for the two extreme cases (for NBI heating only
at 3.1 s and for 2.0 MW of ECRH heating at 8.0 s). Er-
ror bars are given with 2 standard deviations σ for the
fitted profiles and only 1σ for the corresponding gradi-
ents. Values at mid-radius, where the modelling effort
is performed, are underlined. It is found that, at this
radial location, R/L_{T_i} and u' are larger in the case of
NBI heating only (both parameters are correlated due to
NBI being a source of heat and torque), linking hollow
impurity profiles to possible increased thermo- and roto-
diffusion in this case. Additionally, we note that T_i/T_e is
larger, consistent with stabilised ion temperature gradi-
ent driven turbulence (ITG) and higher R/L_{T_i}. The level
of ITG stabilisation inside $r/a = 0.4$ (not investigated in
this study) can be attributed to electromagnetic effects
and/or fast ions [23, 24].

In this paper, emphasis is given to the impact of the
fast ion population on light impurity transport mod-
elling. This requires the characterisation of the fast ion
parameters (shown in Fig. 4) which are computed from
interpretative power balance analysis using the transport
code ASTRA [25] and the implemented Fokker-Planck
solver [26]. The reconstructed plasma stored energies
(including the fast ion contribution) are in agreement
with diamagnetic measurements within a 15% variation

for all phases considered here. The fast ion tempera-
ture used corresponds to the equivalent temperature for
a Maxwellian distribution: $T_{FI} = (2T_\perp + T_\parallel)/3$ where $T_\parallel$
and $T_\perp$ are the parallel and perpendicular (with respect
to the magnetic field) temperatures of a bi-Maxwellian
distribution function. The choice of a Maxwellian back-
ground for the NBI fast ions is justified by the lack of
sensitivity to more realistic fast ion distribution functions
found in gyrokinetic analysis of JET plasmas [27].

	n_{FI}/n_e	$R/L_{n_{FI}}$	T_{FI}/T_e	$R/L_{T_{FI}}$
Case #1 (3.1 s)	0.13	9.5	15.2	0.73
Case #4 (8.0 s)	0.08	10.5	15.9	0.72

TABLE I: Fast ion parameters obtained from power balance
analysis and the Fokker-Planck solver in the transport code AS-
TRA. Here T_{FI} corresponds to the equivalent temperature for a
Maxwellian distribution.

The fast ions parameters are gathered at mid-radius in
Table I for the two cases at 3.1 s and 8.0 s, denoted case
#1 and #4 respectively. As expected for NBI heating,
the normalised fast ion density gradient is larger com-
pared to the normalised temperature gradient (in con-
trast to cases with ICRH). Case #1 features a large fast
ion concentration even at mid-radius due to the use of an
additional off-axis beam compared to case #4.

III. IMPACT OF THE FAST IONS IN THE MODELLING OF TURBULENT AND NEOCLASSICAL IMPURITY TRANSPORT

In this section, the impact of fast ions on neoclassical
and turbulent modelling of light impurity transport is
scrutinised. All simulations are performed at mid-radius
with the codes NEO [28] for neoclassical transport and
GKW [29] for electromagnetic local turbulence. The im-
pact of fast ions on each component is described sepa-
rately.

A. Methodology for the impurity peaking factor modelling

First, the methodology used in this paper to compute
the impurity peaking factor from neoclassical and gyroki-
netic simulations is briefly recalled. More details can be
found in [3, 4]. The total impurity flux is decomposed as
the sum of a neoclassical and a turbulent flux. The level
of turbulent fluxes can be computed directly from non-
linear flux-matched simulations or deduced from linear
simulations using a quasilinear estimate. In the latter
case, the particle flux is rescaled with the ratio of the
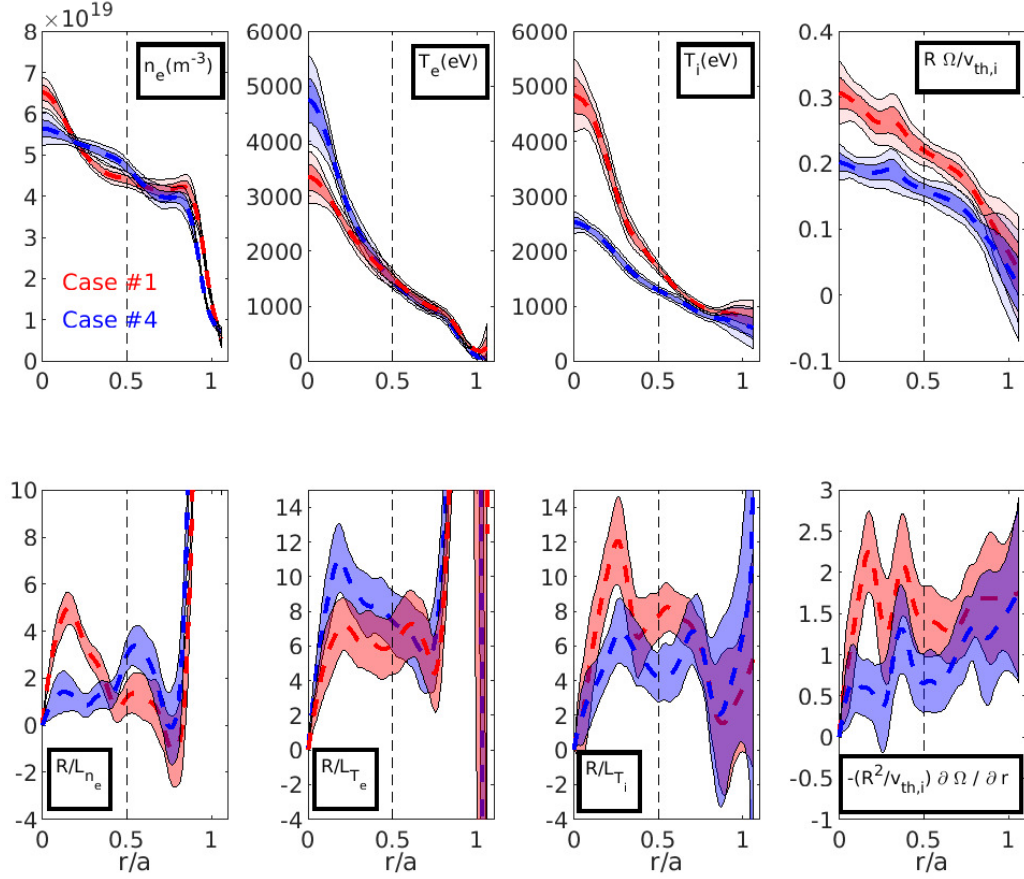anomalous over the turbulent ion heat diffusivity:

FIG. 3: Kinetic profiles (2σ error bars) and corresponding normalised gradients (1σ error bars) for the two stationary phases at 3.1 s (case #1 with 10 MW of NBI) and 8.0 s (case #4 with 7.5 MW of NBI and 2 MW of ECRH).

$$\Gamma_{Z,tot} = \Gamma_{Z,neo} + \frac{\Gamma_{Z,turb}}{\chi_{i,turb}}\chi_{i,an} \qquad (1)$$

Here Z refers to the charge number of the impurity, the subscripts *neo* to the neoclassical part of the particle flux, *turb* to the turbulent part and *an* to the anomalous contribution computed from the power balance $\chi_{i,PB}$ and neoclassical heat diffusivities: $\chi_{i,an} = \chi_{i,PB} - \chi_{i,neo}$. To compute the quasilinear estimate of $\Gamma_{Z,turb}$, linear simulations with poloidal wave numbers ranging from $k_\theta\rho_i = 0.2$ to $k_\theta\rho_i = 0.9$ ($\rho_i = m_i v_{th}/eB$ being the deuterium Larmor radius) and a radial wave number $k_x\rho_i = 0$ are performed. A weight factor is then applied on such spectra to mimic nonlinear features, such as shifts of the maximum perturbed electrostatic potential amplitude to lower wave numbers. This quasilinear approach is relevant for transport studies, in particular due to persistent linear cross-phases between the electrostatic potential and the moments of the perturbed distribution function in the nonlinear regime [30, 31]. Following this approach, linear flux spectra are weighted with

$\gamma_{k_\perp}/<k_\perp^2>$ [30, 32, 33] with $\gamma_{k_\perp}$ the linear growth rate at a given perpendicular wave number and the operator $<>$ defined as:

$$<A> = \frac{\int A|\phi|^2 \mathrm{d}s}{\int |\phi|^2 \mathrm{d}s} \qquad (2)$$

ϕ is the perturbed electrostatic potential along the field aligned coordinate s. Turbulent and neoclassical particle fluxes can be furthermore decomposed into a diffusive and a convective part:

$$\Gamma_Z = \frac{n_Z}{R}D_Z\frac{R}{L_{n_Z}} + n_Z V_Z \qquad (3)$$

with D_Z the diffusion coefficient and V_Z the convective velocity. For the turbulent part, the latter can be decomposed as:

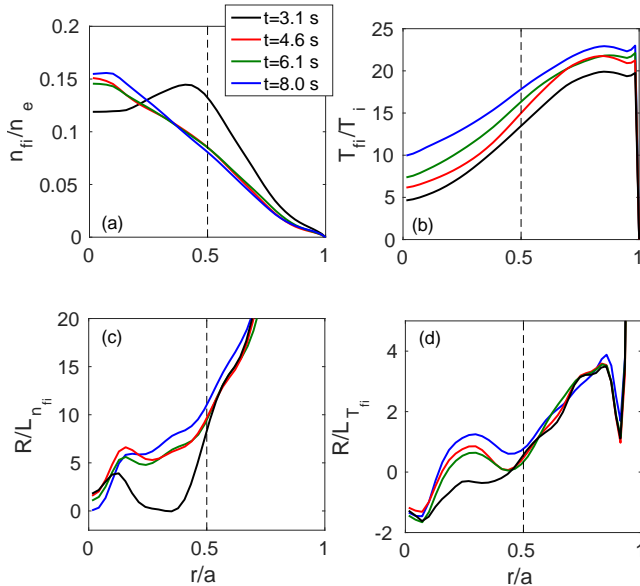$$V_Z = D_Z\left(C_p + C_T\frac{R}{L_{T_z}} + C_u u'\right) \qquad (4)$$

FIG. 4: (a) Density and (b) temperature profiles for the neutral beam fast ions for all phases of Fig. 1. Their corresponding normalised gradients are also shown (c,d).
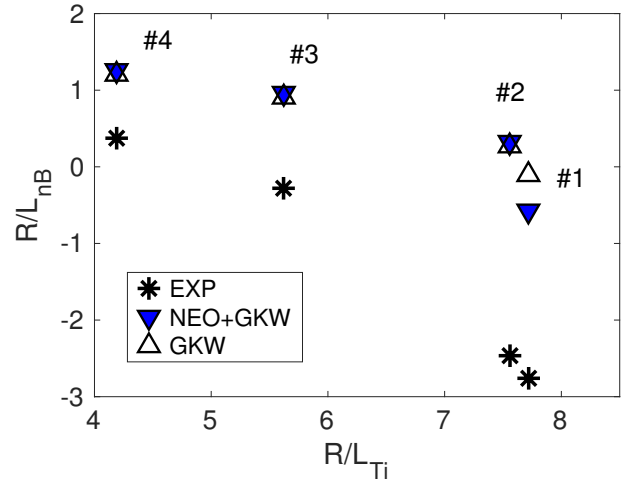

FIG. 5: Experimental and modelled boron peaking factors (without fast ions) versus the normalised ion temperature gradient for the 4 phases of Fig. 1 at $r/a = 0.5$. The modelling assumptions described in section III A were used.

with the constant pinch C_p given by the magnetic field topology, the thermo- and roto-diffusion coefficients C_T and C_u respectively. In steady states (stationary phases) and in the limit of zero impurity source in the core ($\Gamma_{Z,tot} = 0$), the peaking factor R/L_{n_Z} can be deduced from the turbulent and neoclassical transport coefficients as follows:

$$R/L_{n_Z} = -R \frac{\frac{V_{Z,\text{turb}}}{\chi_{i,\text{turb}}} + \frac{V_{Z,\text{neo}}}{\chi_{i,\text{an}}}}{\frac{D_{Z,\text{turb}}}{\chi_{i,\text{turb}}} + \frac{D_{Z,\text{neo}}}{\chi_{i,\text{an}}}} \quad (5)$$

The assumptions and numerical parameters used to compute these impurity transport coefficients are summarised below.

In the gyrokinetic code GKW, collisions are modelled with a pitch-angle scattering operator and electromagnetic effects are kept. The size of the grids used for linear and nonlinear simulations are $n_\mu = 16$, $n_{v_\parallel} = 48$, $n_s/n_{pt} = 40$ for the number of points in the magnetic moment, parallel velocity and parallel direction per poloidal circuit, respectively. The choice of these grids is motivated by linear convergence tests. For nonlinear simulations, the box sizes in the radial x and binormal y directions are 76 ρ_i and 100 ρ_i respectively. The poloidal wave vector is extended to $k_\theta \rho_i = 2$ with 33 modes and $k_x \rho_i$ extends from -11.64 to 11.64 with 339 modes. In these cases, to reduce the computational cost, only four trace impurity species are used (two for each impurity, i.e. boron and helium), thus yielding a diffusive and a convective impurity flux. The latter is not decomposed into the convective coefficients of Eq. 4, in contrast to

linear simulations where 4 traces of the same species are implemented with different background gradients.

In the code NEO, 5 Laguerre and 17 Legendre polynomials are used with the full Fokker-Planck collision operator. In both NEO and GKW, toroidal rotation is included, the magnetic field geometry is constructed from the parametrised Miller geometry [34] and the fast ion population is modelled by a Maxwellian distribution with an equivalent temperature.

With this methodology and assumptions, the quasilinear peaking factor obtained for boron is shown in Fig. 5 together with the experimental values at mid-radius for the four stationary phases depicted in the previous section. This comparison is performed with respect to the normalised ion temperature gradient, where the highest R/L_{T_i} corresponds to the largest value of P_{NBI}/P_{TOT} and the lowest value of R/L_{T_i} to the lowest P_{NBI}/P_{TOT} ratio. The addition of neoclassical transport starts to make a difference for the highest R/L_{T_i} case whereas, for the other cases, its contribution remains negligible compared to turbulent transport. Here, 'standard' modelling was used, that is, with the same theoretical ingredients as in previous publications [3, 4, 11, 13]. In these conditions, the experimental boron peaking factor is increasingly overestimated as the normalised ion temperature gradient increases. This misprediction, observed in [11, 13], was found to be robust against a number of sensitivity studies on the input plasma parameters. This is why the additional mechanisms introduced by the presence of the fast ion population are scrutinised in the following for these particular stationary phases.

Finally it should be noted that, at low R/L_{T_i} neoclassical transport is negligible with respect to the turbulent contributions and becomes relevant only for the largest values of R/L_{T_i}. This is due to changes in the ratio
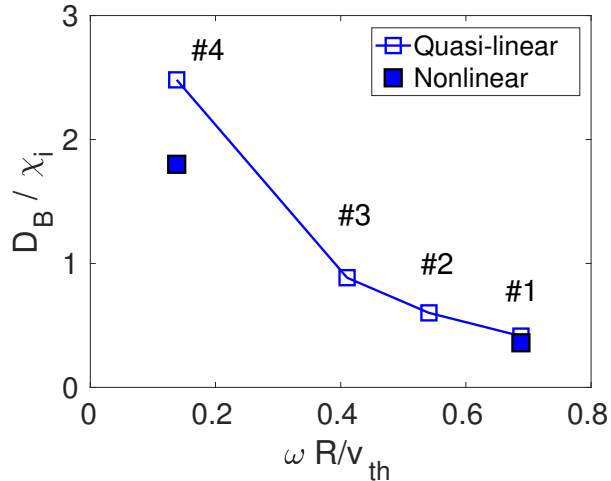
FIG. 6: Ratio of the turbulent boron diffusivity over the turbulent ion heat diffusivity computed from quasi-linear gyrokinetic simulations and shown versus the most linearly unstable normalised mode frequency. Values from nonlinear simulations are also plotted for comparison.

of the turbulent impurity diffusion over the turbulent ion heat diffusivity with increasing fraction of ECRH injected power. Consistently with [35], it is shown in Fig. 6 that D_B/χ_i increases as the most unstable mode frequency decreases and is close to the transition from an ion temperature gradient driven mode (ITG) to a trapped electron mode (TEM) with negative mode frequency (here positive frequencies correspond to the direction of the ion diamagnetic drift). These quasilinear results are also consistent with nonlinear simulations performed for the two extreme cases, namely the phase with 10 MW of NBI heating and no ECRH (phase #1) and the phase with 7.5 MW of NBI heating and 2 MW of ECRH (phase #4). The change in the turbulent D_B/χ_i is directly connected to the relative strength of the neoclassical transport coefficients. For the highest R/L_{T_i} case, a significantly lower value of D_B/χ_i is obtained, which results in an increased importance of the neoclassical convection. However, this effect alone cannot reproduce the observed hollowness of the experimental profiles.

B. Fast ions and turbulent impurity transport

Fast ions are known to stabilise ITG turbulence linearly and nonlinearly [23, 36, 37] due to dilution, resonant effects in the velocity space and electromagnetic contributions characterised by the normalised plasma pressure $\beta = 2\mu_0 nT/B^2$ which increases with the fast ions pressure.

The same gyrokinetic simulations as in Fig. 5 are performed with fast ions and the turbulent helium and boron peaking factors are now shown in Fig. 7 top panels. To characterise the impact of fast ions on the turbulent
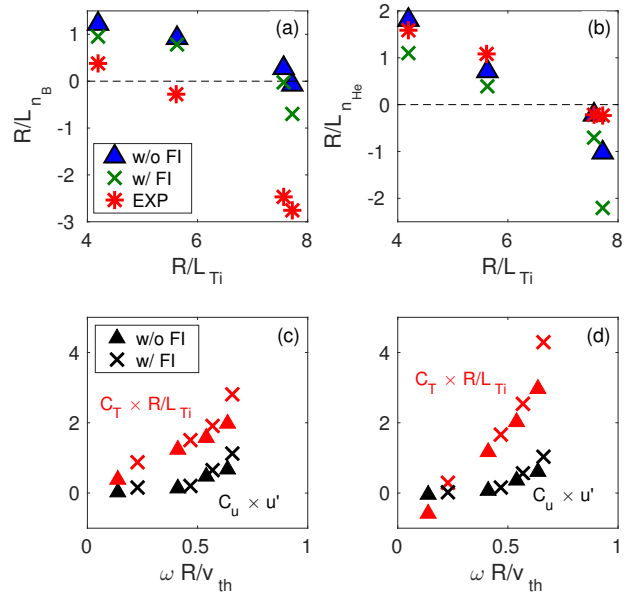

FIG. 7: (Top panels) Boron and helium turbulent peaking factors for the four studied phases (neoclassical transport is not considered here). Quasilinear results ($k_\theta \rho_i = 0.2 - 0.9$) with or without fast ions are compared to experimental measurements. (Bottom panels) Contributions from the different convective terms in the computed quasilinear boron (c) and helium (d) peaking factors.

transport only, neoclassical contributions are not considered in this section.

Throughout the variation of R/L_{T_i} the impact of fast ions on the turbulent boron peaking factor results in lower R/L_{n_B} with a stronger effect for the high R/L_{T_i} case (10 MW of NBI power). Even in this regime, the effect on the turbulent transport alone is small compared to the experimental values observed but comparable to neoclassical contributions. In contrast, for the turbulent helium peaking factors, a significant decrease is observed for the whole range of normalised temperature gradient values, resulting in additional discrepancies with experimental levels.

The relative strength of the different convective mechanisms is shown in the bottom panels of Fig. 7 where the quasilinear coefficients of Eq. 4 are plotted against the normalised mode frequency (ω) at $k_\theta \rho_i = 0.3$. Increasing positive ω values (ITG turbulence) also corresponds to increasing R/L_{T_i} and u'. Unsurprisingly, turbulent outward convection driven by the ion temperature gradient and the toroidal rotation gradient also increase. The relative strength of roto-diffusion (A/Z dependency) is larger for boron than for helium due to the large fraction of outward thermo-diffusion for the latter (1/Z dependency). Including fast ions results in an increase of both convective mechanisms which yields the reduced peaking factors shown in the top panels.

To characterise the effect of fast ions on the impurity peaking factors, linear simulations without fast ions
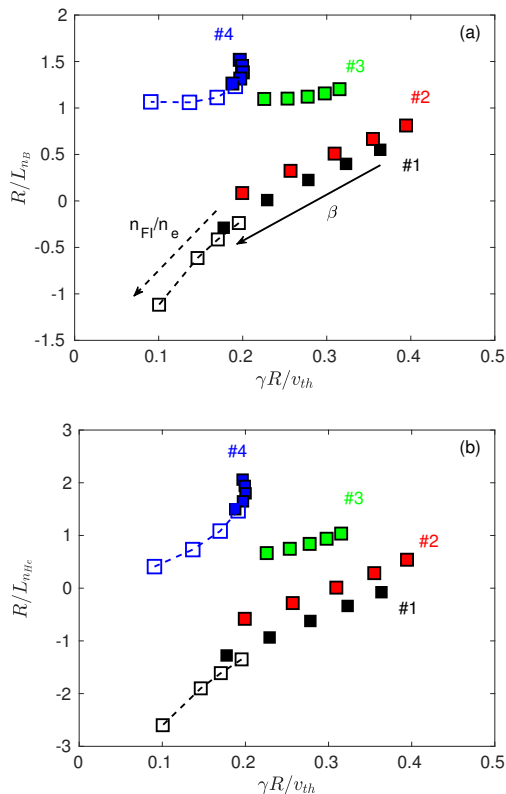
FIG. 8: Comparison of the electromagnetic and fast ion effects on linear ($k_\theta \rho_i = 0.3$) growth rates stabilisation and light impurity peaking factors for the 4 phases of Fig. 1. The increasing values of the fast ion concentration and β are indicated by the dashed and solid arrows respectively. n_{FI}/n_e is varied from -20% the nominal value to $n_{FI}/n_e = 0.2$. β ranges from 0.1% to 0.9%.

at $k_\theta \rho_i = 0.3$ are performed, with increasing reference plasma pressures $\beta_{ref} = 2\mu_0 n_e T_i / B^2$ from 0.1% to 0.9% as it is known that electromagnetic effects can affect significantly the predicted impurity peaking factor [38]. All other parameters are kept at their nominal values. It is shown in Fig. 8 that the predicted impurity peaking factors are correlated with the ITG stabilisation by electromagnetic effects. For strong linear stabilisation with β_{ref} up to 0.9%, strong reduction of R/L_{n_z} is obtained due to increased outward convection, in particular for the large ω and R/L_{T_i} cases.

Simulations including fast ions for case #1 and #4 using the nominal parameters of table I and changing the fast ion content from -20% the nominal n_{FI}/n_e to $n_{FI}/n_e = 0.2$ can now be compared to the changes in β_{ref}. Interestingly the impact of fast ions on the impurity peaking factors is also correlated to the mode stabilisation in particular in cases of strong convection (case #1 with 10 MW NBI case). In contrast, for the case at 8.0 s (case #4 with 7.5 MW of NBI and 2 MW of ECRH), further stabilisation is obtained with relatively no effect on the boron peaking factor whereas $R/L_{n_{He}}$ is still clearly affected. This is explained by the larger variation of the

helium thermo-diffusion C_T compared to boron.

Knowing that fast ions have an increased impact on nonlinear ITG turbulence, nonlinear simulations are required to characterise their complete effect on the light impurity peaking factor. These simulations can be particularly difficult to perform due to electromagnetic fast ion modes which can completely quench the turbulence yielding unrealistic heat fluxes. Several ways to circumvent this problem are used in the literature, such as using increased magnetic shear, decreased safety factor or reducing the driving terms of these electromagnetic fast ion modes (e.g. $R/L_{n_{FI}}$) [39]. It was found in sensitivity studies performed with linear simulations that n_{FI}/n_e and $R/L_{n_{FI}}$ are the most relevant parameters regarding quantitative variations of the impurity peaking factors whereas T_{FI}/T_e has minor effects. Thus we chose to reduce this term to $T_{FI}/T_e = 11.1$ and $T_{FI}/T_e = 13.3$ for case #1 and #4. This corresponds to a relative reduction of $\sim 27\%$ and 16% with respect to the nominal values $T_{FI}/T_e = 15.2$ and $T_{FI}/T_e = 15.9$ respectively. This change of fast ion temperatures shifts the peak of the resulting unstable mode to higher $k_\theta \rho_i$ where it is stabilised. Finally, unless stated otherwise, all nonlinear simulations include $E \times B$ shearing as it is expected to have an impact on turbulent impurity convection via symmetry breaking of the gyrokinetic equations [4].

The saturated nonlinear ion heat fluxes for case #1 (10 MW of NBI heating and no ECRH) and case #4 (7.5 MW of NBI heating and 2 MW of ECRH heating) are shown in Fig. 9. In both cases, fast ions significantly reduce the predicted ion heat flux down to the experimental levels (computed from power balance analysis). The reduction is particularly large for the 10 MW NBI case where the ion heat flux predicted without fast ions is a factor 9 larger. Matching experimental heat fluxes is mandatory for impurity transport predictions as one does not require the rescaling of the turbulent fluxes used in Eq. 5 to consistently include neoclassical transport. Despite the reduction of T_{FI}/T_e discussed previously, two phases can be identified for case #1. A first phase, where the predicted heat flux is in quantitative agreement with power balance analysis and a second phase where the heat flux is strongly reduced to much lower levels. This transition also observed in [37] and described as nonlinear interactions between fast particle driven modes, ITG and zonal flows is not further investigated as the relevance of such simulations with respect to experimental ion heat flux levels remains questionable.

The turbulent impurity peaking factors for the cases #1 and #4 are gathered in Fig. 10 for both helium and boron. It is found that the reduction of the nonlinear boron and helium peaking factors when fast ions are included, are quantitatively consistent with quasilinear predictions for case #4. Regarding case #1, during the first phase where ion heat fluxes are matched to the power balance levels, the reduction in the nonlinear $R/L_{n_{He}}$ is also consistent with quasilinear predictions. On the other hand, no sizable changes are observed for
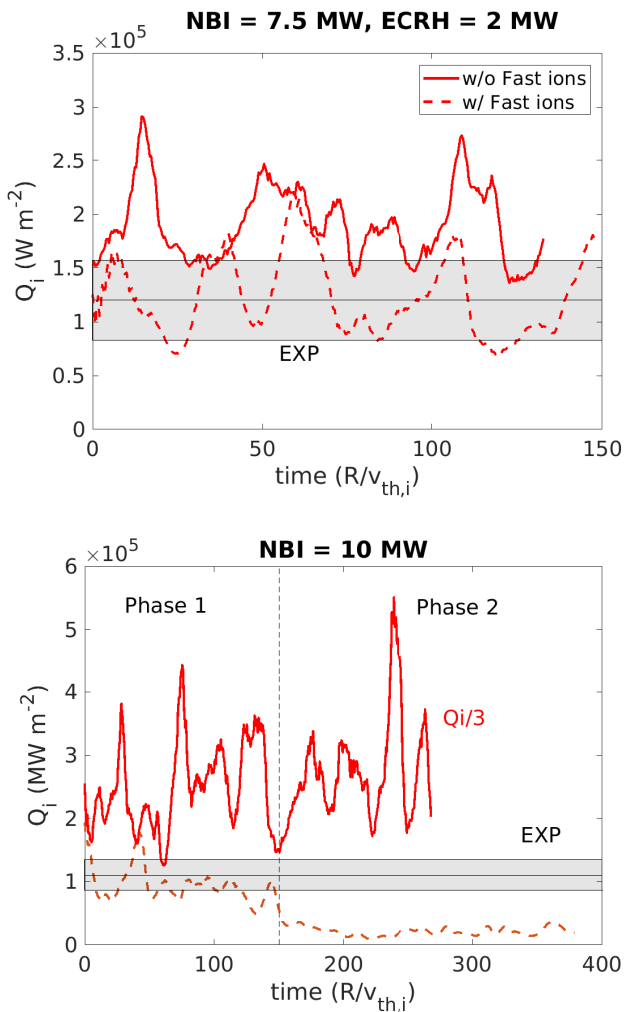
FIG. 9: Saturated ion heat flux from nonlinear simulations with and without fast ions versus the time in units of $R/v_{th,i}$. Comparisons with the experimental heat flux are performed for the two extreme cases at $t = 8.0s$ (case #4 top panel) and $t = 3.1s$ (case #1 bottom panel).
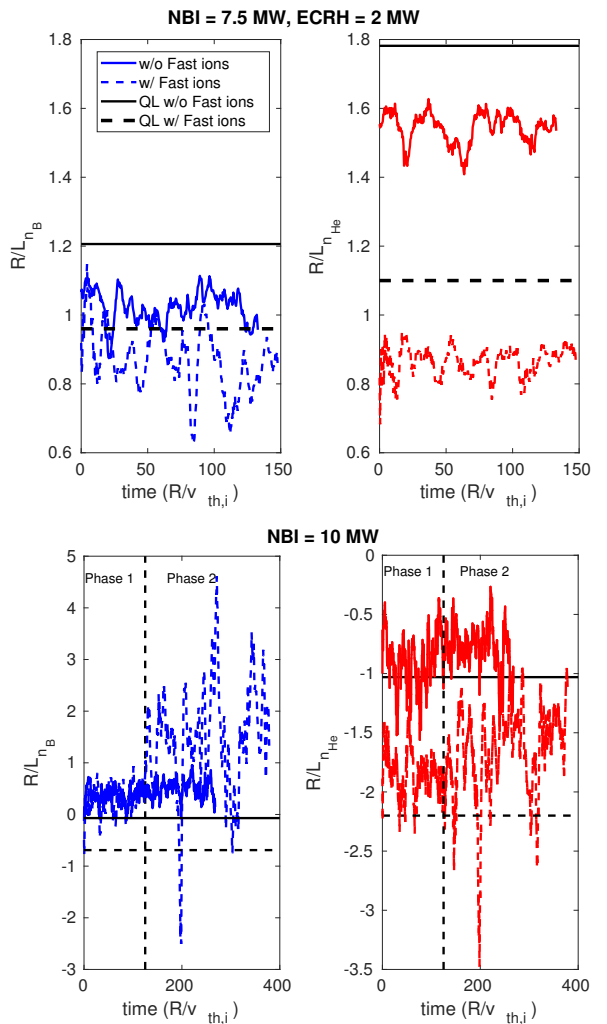

FIG. 10: Nonlinear impurity peaking factors from simulations with and without fast ions for case #4 (top panels) and case #1 (bottom panels) versus the time in units of $R/v_{th,i}$. Quasi-linear predictions are also shown.

the nonlinear boron peaking factor. During the second phase, where ion heat fluxes are not matched anymore, large variations of both helium and boron peaking factors are obtained, with mean values for boron departing from the experimental levels, adding more inconsistencies.

Additional simulations with increased $R/L_{T_i} = 8.5$ and $u' = 2$ (nominal values are $R/L_{T_i} = 7.7$ and $u' = 1.4$) have been performed for case #1 to test the strength of the fast ion effect on the nonlinear boron peaking factor and assess the role of $E \times B$ shearing. The results are shown in Fig.11. In this case, the predicted heat flux is a factor two larger than the experimental level. Moreover, no more transitions are observed as in Fig. 9 bottom panel and the heat flux level remains stationary on average. In these conditions, the boron peaking factor is decreased with fast ions, going from -0.02 to -0.42. The impact of $E \times B$ shearing, summarised in Tab. II, is found

to have opposite effects (though small) with and without fast ions. Without fast ions, the addition of $E \times B$ shearing results in less hollow predicted impurity profiles whereas with fast ions, R/L_{n_B} and $R/L_{n_{He}}$ are both reduced (more hollow).

	B		He	
	w/o FI	w/ FI	w/o FI	w/ FI
w/ $E \times B$	-0.02	-0.42	-1.19	-2.31
w/o $E \times B$	-0.04	-0.31	-1.27	-2.27

TABLE II: Nonlinear peaking factors for case #1 at $R/L_{T_i} = 8.5$ and $u' = 2$.

Nonlinear simulations of the turbulent impurity peaking in presence of fast ions are particularly expensive and sensitive to additional parameters (fast ion background).
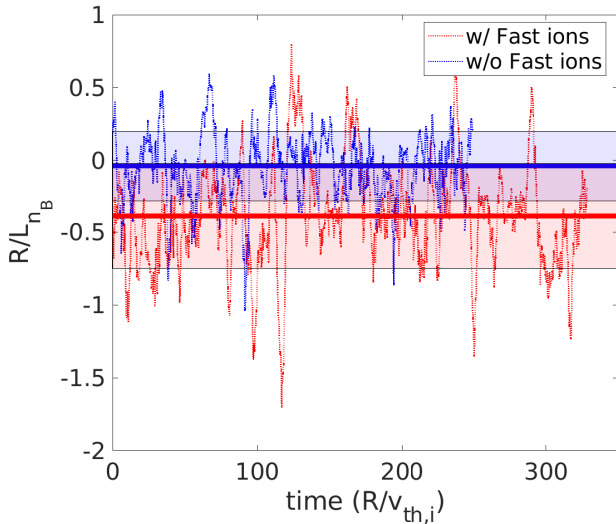
FIG. 11: Boron peaking factors for nonlinear simulations with and without fast ions, including $E \times B$ shearing for case #1. Higher values of $R/L_{T_i} = 8.5$ and $u' = 2$ are used as described in the text. Mean values with one standard deviation (shaded areas) are also indicated for both simulations.

Here it is shown that the levels of peaking factor reductions observed in quasilinear simulations are quantitatively consistent with nonlinear simulations minus the complexity (fast particle driven mode, $E \times B$ shearing). This is particularly interesting for database analysis, including the additional contributions from fast ions.

C. Fast ions and neoclassical transport

In presence of fast ions, light impurity neoclassical transport is modified in two ways. One is indirect and comes from the relative neoclassical transport weight compared to turbulent impurity fluxes due to reductions in D_Z/χ_i. The other is from direct changes of neoclassical convection due to changes in R/L_{n_i} from quasi-neutrality when fast ions are included.

Firs, the turbulent ratio D_Z/χ_i is computed for an increasing fraction of fast ions (n_{FI}/n_e in Fig. 12 at $k_\theta \rho_i = 0.3$. It is observed that for both boron and helium, D_Z/χ_i decreases with increasing concentrations of fast ions. Following Eq. 5, the decrease of D_Z/χ_i results in an increasing fraction of the neoclassical contribution to the total impurity peaking factor. The decrease of the boron D_B/χ_i with the fast ion concentration quantitatively agrees with nonlinear simulations which again supports the use of quasi-linear analysis.

In the following, the neoclassical transport for boron including fast ions is studied, due to the negligible contribution observed for helium (even with the reduced turbulent $D_{Z,\text{turb}}/\chi_{i,\text{turb}}$). The additional fast ion density modifies the light impurity neoclassical transport in two ways: first, the modification of the background main ion
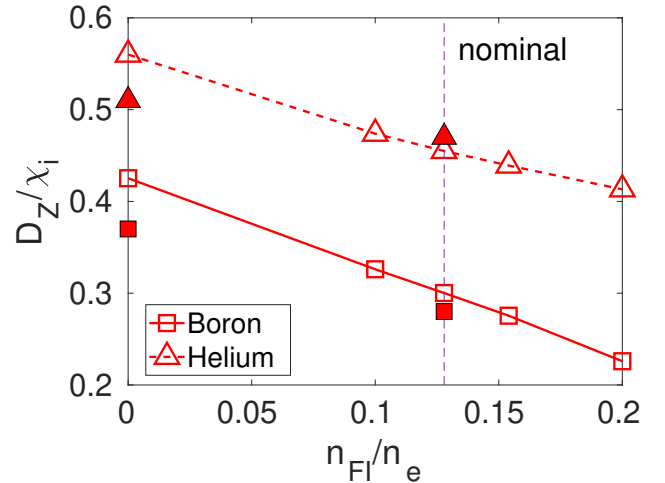

FIG. 12: Turbulent D_Z/χ_i computed at $k_\theta \rho_i = 0.3$ with increasing fraction of fast ions in the 10 MW NBI heated case. The open symbols correspond to linear results, while the nonlinear results are indicated with full symbols (only phase 1 of Fig. 9 has been used).

density gradient from quasi-neutrality and second, the friction between impurities or main ions and fast ions. These two mechanisms act in opposite directions. The reduced main ion density gradient results in a decreased inward neoclassical convection but the ion/fast ion friction neoclassical flux has an additional inward contribution. To disentangle these two mechanisms, the role of the change in R/L_{n_i} is underlined in Fig. 13. Starting from the parameters of the 10 MW NBI heated case, a scan in R/L_{n_i} is performed without fast ions (blue symbols). Then the latter are added and their normalised density gradient is increased at constant concentration, such that the resulting R/L_{n_i} is modified by quasineutrality (red symbols). Finally this scan is repeated and the ion/fast ion friction force is artificially removed (black symbols).

It is found that the reduction of R/L_{n_i} due to the presence of fast ions when ion/fast ions friction is removed, increases the outward convection of boron in the same way as changing directly R/L_{n_i}. In contrast when all friction terms are properly included, the increase in the convection is lower with increasing positive values of $R/L_{n_{FI}}$.

IV. COMPARISONS OF EXPERIMENTAL AND MODELLED PEAKING FACTORS

In this section, all mechanisms investigated in the previous sections and related to the fast ion population, are put together and the predicted total impurity peaking factors using Eq. 5 are compared to experimental values.

Each of the mechanisms, is individually separated in Fig. 14 for the 10 MW NBI heated case (#1), using quasi-linear gyrokinetic simulations ($k_\theta \rho_i = 0.2 - 0.9$).
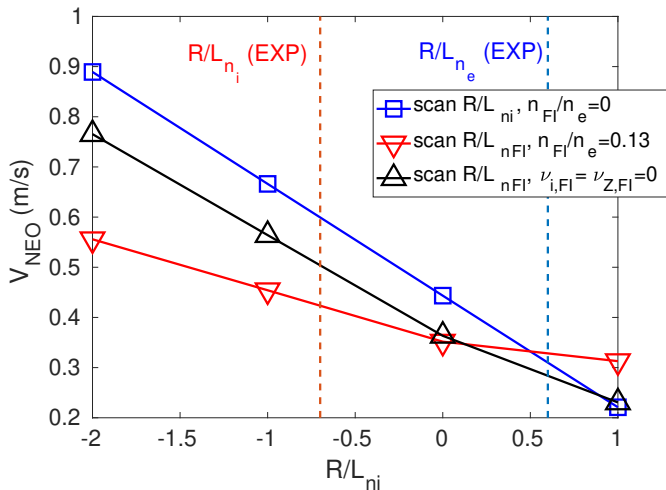
FIG. 13: Neoclassical convection due to changes in the main ion normalised density gradient with (red) or without fast ions (blue). The fast ion density gradient is increased at constant fast ion concentration to change R/L_{n_i} from the quasi-neutrality constraint. Neoclassical simulations without ion/fast ions friction are also performed (shown in black). Nominal values for R/L_{n_i} without fast ions and with fast ions are shown with vertical blue and red dashed lines respectively.

FIG. 15: Boron peaking factors computed for case #1 at $r/a = 0.5$ with variations, around their nominal values, of several important parameters regarding impurity transport (the nominal value used for T_e/T_i is 0.93). Modelled R/L_{n_B} include both neoclassical and turbulent transport, without and with fast ions (blue and red solid lines respectively). The experimental value is also indicated in each plot by the black solid lines.
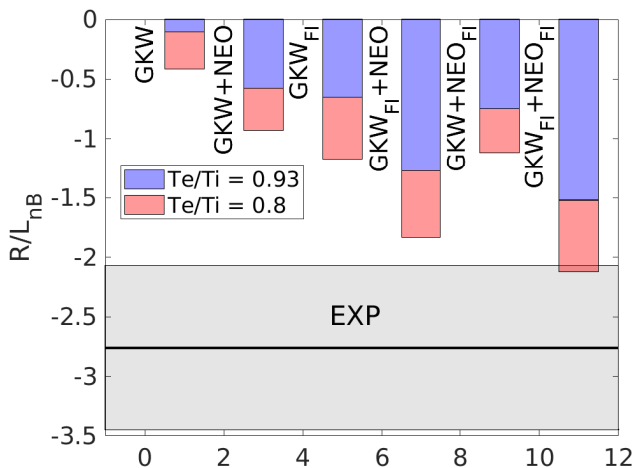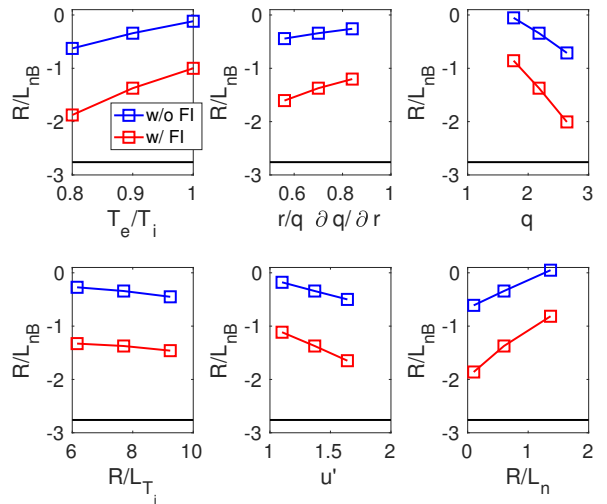

FIG. 14: Comparison of the modelled boron peaking factors predicted with different assumptions on neoclassical and turbulent contributions. The subscript FI refers to the inclusion of fast ions in the corresponding transport codes. Results are shown for the nominal value of $T_e/T_i = 0.93$ and a reduced value $T_e/T_i = 0.8$. A 25 % variation of the experimental R/L_{n_B} is also indicated by the gray band.

While the additional mechanisms stemming from the inclusion of fast ion population are included, all other parameters are kept fixed. As already observed, the effect of fast ions on turbulent transport alone is not particularly strong with respect to experimental values of R/L_{n_B}. Still it is of the same order as the neoclassical contribution (without fast ions). Including neoclassical transport

without fast ions on top of linear gyrokinetic simulations with fast ions results in another decrease of R/L_{n_B}. This is due to the combination of the increased turbulent convection but also to the increase of the neoclassical contribution through the decrease of the turbulent D/χ_i with fast ions. A similar analysis is done now with decreased T_e/T_i as this is one of the important parameters in determining the impurity peaking. It is found that with $T_e/T_i = 0.8$ (at the limit of the 1σ error bars of Fig. 3), the predicted peaking factor with fast ions falls now inside a 25 % variation of the experimental peaking factor.

This underlines the fact that all these mechanisms provide a decrease of R/L_{n_B} by a significant amount and that peaking factor predictions are now very sensitive to input parameters allowing even closer match with experimental measurements. This sensitivity to plasma parameters is further studied in Fig. 15 where the variations of R/L_{n_B} with T_e/T_i, the magnetic shear, the safety factor, R/L_{T_i}, u' and R/L_n are computed from linear simulations at $k_\theta \rho_i = 0.3$. The variations of these parameters around their nominal values are taken into account in both the neoclassical and linear gyrokinetic simulations. The power balance ion heat flux is kept fixed, resulting in changes for $\chi_{i,\text{PB}}$ only with T_i and R/L_{T_i}. Error bars on the deposited power and corresponding ion heat flux is not considered and could be another source of uncertainties on the predicted R/L_{n_Z}. Overall the absolute changes in R/L_{n_B} are larger when fast ions are included. The parameters providing the largest variations of the boron peaking factors are T_e/T_i, R/L_n and q.

Results on the helium peaking factors including fast ions (neoclassical transport being negligible) showed that
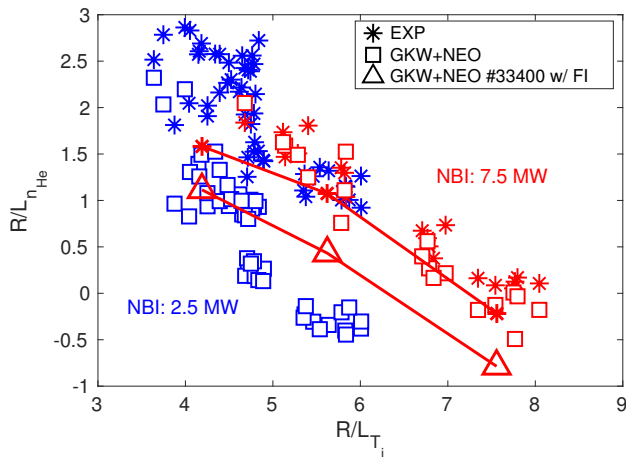
FIG. 16: Comparisons of the experimental (stars) and modelled (squares) helium peaking factors against the normalised ion temperature gradients from previous experimental and modelling results [11]. The $R/L_{n_{He}}$ predictions including fast ions from this work are shown as red triangles and the corresponding experimental points as the red line with red stars.

turbulent thermo-diffusion is increased in the whole range of R/L_{T_i} studied here and results in a systematic decrease of $R/L_{n_{He}}$. To put this result in perspective with previous work including 2.5 and 7.5 MW NBI heated plasmas, Fig. 12(b) of [11] is reproduced in Fig. 16 together with results obtained in this work for the cases with 7.5 MW of NBI. It was shown that without fast ions, there is an offset in the modelled $R/L_{n_{He}}$ between 2.5 and 7.5 MW NBI heated cases whereas experimental $R/L_{n_{He}}$ linearly decreases with increasing R/L_{T_i}. Including fast ions tends to reduce the offset in the modelling which makes the predicted peaking factors more consistent with the experimental qualitative trend with R/L_{T_i}. Still a systematic underprediction of the experimental helium peaking factor remains to be explained.

V. CONCLUSIONS

A selected discharge performed at ASDEX Upgrade, where modelling predictions for boron profiles fail to describe the experiment, in particular in the condition of large NBI heating compared to ECRH heating, is further investigated by means of extensive gyrokinetic and neoclassical simulations. This discharge features high levels of neutral beam ion heating and for this reason, a strong emphasis is given to the impact of fast ions on impurity transport. Not including fast ions results in strongly overpredicted R/L_{n_B} at mid-radius ($R/L_{n_B} = -0.6$) compared to experimental values ($R/L_{n_B} = -2.7$). As largely documented in the literature, the experimental ion heat flux is also overestimated in the absence of fast ions. On the other hand, the helium peaking factor is

correctly predicted without fast ions for this high NBI power heated discharge but features a systematic underprediction for previous lower NBI heated discharges in [11].

The newly described impact of an equivalent Maxwellian background fast ion population on the prediction of the light impurity peaking factor R/L_{n_Z} is found to be a combination of several effects. In linear and nonlinear gyrokinetic simulations, it is shown that fast ions increase the turbulent outward convection of light impurities. This is similar to electromagnetic effects [38] in the sense that there is a strong correlation between predicted R/L_{n_Z} and linear ion temperature gradient mode stabilisation. For strong stabilisation, quasilinear outward impurity convective terms, namely the roto- and thermo-diffusion are increased yielding hollow profile predictions for boron but still outside the experimental values. The same increased outward convection is observed for helium with a relatively stronger thermo-diffusion term compared to roto-diffusion. In addition to increasing the turbulent outward convection, the ratio of the impurity diffusivity over the ion heat diffusivity D_Z/χ_i is decreased when fast ions are included. This ratio is particularly important to properly include neoclassical transport to quasi-linear gyrokinetic simulations using power balance analysis to force the saturation amplitude at experimental levels. While neoclassical transport usually provides small contributions to light impurity transport from mid-radius outwards and can be often neglected, it is shown here that in conditions of dominant ion heating and in the presence of fast ions, which lead to relatively small values of D_Z/χ_i, neoclassical convection can become significant. Finally, this convection is also modified when fast ions are included, as the main ion density gradient responsible for the neoclassical inward convection changes. Friction between ions and fast ions acts in the opposite way with an additional inward pinch. The resulting neoclassical convection is dominated by changes in R/L_{n_i} yielding larger outward neoclassical convective velocities with fast ions.

The combination of these effects stemming from the inclusion of fast ions in gyrokinetic and neoclassical light impurity transport simulations are mandatory to reproduce experimental hollow boron profiles and experimental ion heat fluxes. On the other hand the helium peaking factor is now underpredicted in high NBI heated plasmas due to the increased outward turbulent thermo-diffusion (neoclassical helium transport is negligible even when fast ions are included). Such underpredictions have also been observed in low NBI heated phases and could hint toward a more general mechanism responsible for systematic underprediction of the helium peaking factor.

[1] C. Angioni and A. G. Peeters, Physical Review Letters **96**, 095003 (2006)

[2] Y. Camenen, A. G. Peeters, C. Angioni, F. J. Casson, W. A. Hornsby, A. P. Snodin, and D. Strintzi, Physics of Plasmas **16**, 012503 (2009)

[3] C. Angioni, R. M. McDermott, E. Fable, R. Fischer, T. Pütterich, F. Ryter, G. Tardini, and the ASDEX Upgrade Team, Nuclear Fusion **51**, 023006 (2011)

[4] F. Casson *et al*, Nuclear Fusion **53**, 063026 (2013)

[5] H. Nordman *et al*, Plasma Physics and Controlled Fusion **53**, 105005 (2011)

[6] A. Skyman, L. Fazendeiro, D. Tegnered, H. Nordman, J. Anderson, and P. Strand, Nuclear Fusion **54**, 013009 (2013)

[7] D. R. Mikkelsen *et al*, Physics of Plasmas **21**, 082302 (2014)

[8] N. T. Howard *et al*, Nuclear Fusion **52**, 063002 (2012)

[9] C. Angioni *et al*, Nuclear Fusion **54**, 083028 (2014)

[10] F. J. Casson *et al*, Plasma Physics and Controlled Fusion **57**, 014031 (2015)

[11] A. Kappatou *et al*, Nuclear Fusion **59**, (2019)

[12] N. Bonanomi, P. Mantica, C. Giroud, C. Angioni, P. Manas, S. Menmuir and JET Contributors, Nuclear Fusion **58**, 036009 (2018)

[13] P. Manas, Y. Camenen, S. Benkadda, H. Weisen, C. Angioni, F. J. Casson, C. Giroud, M. Gelfusa, M. Maslov and JET contributors, Physics of Plasmas **24**, 062511 (2017)

[14] Y. Nakamura *et al*, Nuclear Fusion **57**, 056003 (2017)

[15] C. Bruhn *et al*, Plasma Physics and Controlled Fusion **60**, 085011 (2018)

[16] C. Bruhn *et al*, Plasma Physics and Controlled Fusion (Erratum), *to be submitted*

[17] A. Kappatou *et al*, Plasma Physics and Controlled Fusion **60**, 055006 (2018)

[18] C. Angioni, Y. Camenen, F. J. Casson, E. Fable, R. M. McDermott, A. G. Peeters, and J. E. Rice, Nuclear Fusion **52**, 114003 (2012)

[19] R. M. McDermott *et al*, Plasma Physics and Controlled Fusion **53** 035007 (2011)

[20] R. M. McDermott *et al*, Plasma Physics and Controlled Fusion **60** 095007 (2018)

[21] A. Bortolon, Y. Camenen, A. N. Karpushov, B. P. Duval, Y. Andrebe, L. Dederspiel, O. Sauter, and the TCV Team, Nuclear Fusion **53**, 023002 (2013)

[22] P. McCarthy, Physics of Plasmas **6**, 3554 (1999)

[23] J. Citrin *et al*, Physical Review Letters **111**, 155001 (2013)

[24] F. Ryter *et al*, Nuclear Fusion **59**, 096052 (2019)

[25] G. V. Pereverzev, P. N. Yushmanov, IPP-Report, IPP 5/98 (2002)

[26] A. Polevoi, H. Shirai and T. Takizuka, JAERI-Data/Code 97-014, March 1997

[27] A. Di Siena, T. Goerler, H. Doerk, R. Bilato, J. Citrin, T. Johnson, M. Schneider, E. Poli, and JET Contributors, Physics of Plasmas **25**, 042304 (2018)

[28] E. Belli, J. Candy, Plasma Physics and Controlled Fusion **51**, 075018 (2009)

[29] A. G. Peeters, Y. Camenen, F. J. Casson, W. A. Hornsby, A. P. Snodin, D. Strintzi, G. Szepezi, Computer Physics Commnunications **180**, 2650 (2009)

[30] T. Dannert and F. Jenko, Physics of Plasmas **12**, 072309 (2005)

[31] A. Casati *et al*, Nuclear Fusion **49**, 085012 (2009)

[32] M. Kotschenreuther, W. Dorland, M. A. Beer, and G. W. Hammett, Physics of Plasmas **2**, 2381 (1995)

[33] F. Jenko, T. Dannert, and C. Angioni, Plasma Physics and Controlled Fusion **47**, B195 (2005)

[34] R. L. Miller, M. S. Chu, J. M. Greene, Y. R. Lin-Liu and R. E. Waltz, Physics of Plasmas **5**, 973 (1998)

[35] C. Angioni, Physics of Plasmas **22**, 102501 (2015)

[36] A. Di Siena, T. Goerler, H. Doerk, E. Poli and R. Bilato, Nuclear Fusion **58**, 054002 (2018)

[37] A. Di Siena *et al*, Nuclear Fusion **59**, 124001 (2019)

[38] T. Hein and C. Angioni, Physics of Plasmas **17**, 012307 (2010)

[39] J. Citrin *et al*, Plasma Physics and Controlled Fusion **57** 014032 (2015)